Supporting Information

Title: Aggregation-triggering segments of SOD1 fibril formation support a common pathway for familial and sporadic ALS

Authors: Magdalena I Ivanova, Stuart A Sievers, Elizabeth L. Guenther, Lisa M. Johnson, Duane D. Winkler, Ahmad Galaleldeen, Michael R Sawaya, P. John Hart, David Eisenberg[1]
[1]Corresponding author:
Howard Hughes Medical Institute,
UCLA-DOE Institute for Genomics and Proteomics,
Department of Biological Chemistry, UCLA,
Los Angeles CA 9095-1570
Email: david@mbi.ucla.edu
Phone: 310 825-3754

SI Materials and Methods:

Peptide synthesis: **^{147}GVIGIAQ^{153}**, **^{14}VQGIINFE^{21}**, **^{33}GSIKGL^{38}**, and **^{101}DSVISLS^{10}** were purchased from CS Bio and Celtek Bioscience Peptides. GIIGIAQ (V148I) and GVTGIAQ (I149T) were purchased from GenScript.

The rest of the peptides were synthesized on HMPB-ChemMatrix resin using standard Fmoc solid-phase synthesis conditions (1). 200 μmoles of the first amino acid was coupled to 50μmoles of HMPB-ChemMatrix resin with 200 μmoles coupling reagent 1-(Mesitylene-2-sulfonyl)-3-nitro-1H-1,2,4-triazole (MSNT) and 100μl of the base N-methyl-imidazole dissolved in 3ml of dichloromethane. The reaction was capped and left at room temperature overnight. For a coupling step of the rest of the amino acids, 200 μmoles of Fmoc-protected amino acid (4 eq) and coupling reagent O-Benzotriazole-N,N,N',N'-tetramethyl-uronium-hexafluoro-phosphate (HBTU, 4 eq) were weighed into 15ml falcon tube. The amino acid was dissolved in 3.0 ml of 0.1 M 2-(1H-benzotriazole-1-yl)-1,1,3,3-tetramethyluronium hexafluorophosphate (HOBT) in N-methylmorpholine and 135 μl N,N-diisopropylethylamine (DIEA). This mixture was vortexed briefly and allowed to react for at least 1 min. The activated amino acid solution was then added to the fritted/washed polypropylene tube containing the resin. The reaction was heated to 70°C in the Pierce Reacti-Therm heat block for 15min with stirring. After the coupling reaction, the resin was washed three times with dimethyl formamide (DMF). For Fmoc deprotection, 3 ml of 20% piperidine in DMF was added to the resin. The mixture was heated to 70°C in the Pierce Reacti-Therm heat block for 5 min with stirring. After the deprotection reaction, the resin was washed three times with DMF. The cycles of coupling and deprotection were alternately repeated to give the desired full-length peptide. After the final deprotection, the resin was washed three times in DMF followed by three times in dichloromethane and left to dry overnight. Acid-labile side-chain protecting groups were globally removed and peptides were cleaved from the resin by adding 50 μL triisopropylsilane and 50 μL water followed by adding of 4ml trifluoroacetic acid (TFA). The reaction was stirred for three hours. After three hours, the TFA mixture containing the newly synthesized peptides was dripped into a 50ml tube, and the TFA was evaporated overnight in the fume hood.

Peptide purification: After the synthesis the crude peptides were dissolved in 20% to 30% acetonitrile. Peptides were purified on a preparative C18 column (10μm, 250x20mm, Higgins Analytical) using Reverse Phase HPLC with 9ml/min flow rate. Solvent A was 0.1% TFA

dissolved in water. Solvent B was 0.1% TFA dissolved in acetonitrile. The gradient used for peptide purification was 0% to 50% solvent B over 50 minutes. The purity of the synthesized peptides was assessed by C18 analytical column (5μm 250x4.6mm Higgins Analytical) at a flow rate of 1 mL/min and gradient 10-60% B solvent over 50 minutes. Masses of the newly synthesized peptides were verified by MALDI-TOF-MS.

Peptide fibril formation: ^{14}VQGIINFE^{21}, ^{101}DSVISLS^{107} and their corresponding mutants were dissolved in water to a final concentration of 2mM. ^{147}GVIGIAQ^{153} and its corresponding mutants except for ^{147}RVIGIAQ^{153} (G147R) and ^{147}GVTGIAQ^{153} (I149T) were dissolved in water to a final concentration of 1mM. ^{147}GVTGIAQ^{153} (I149T) formed fibril-like aggregates only at 6mM concentration in water. ^{147}RVIGIAQ^{153} (G147R) formed fibrils when dissolved to 1mM in 25mM K phosphate pH 7.0 and 1mM EDTA. Due to the high peptide solubility, ^{30}KVWGSIKGL^{38} and its mutants were dissolved with 0.1M Tris base (pH was not adjusted) to 60 mM. Peptide segments were incubated at 37°C with shaking level 9 in a Torrey Pine Scientific shaker. After 7 to 10 days the samples were examined by transmission electron microscope (TEM).

Crystallization: ^{147}GVIGIAQ^{153} was crystallized using the hanging drop vapor diffusion method: 1 μL of 0.3 mg/mL ^{147}GVIGIAQ^{153} was mixed with 1 μL of reservoir solution. The reservoir solution comprised 1 mL of 1 M sodium acetate pH 4.5 and 1.75 M ammonium sulfate. ^{147}GVTGIAQ^{153} (I149T) was crystallized using the hanging drop vapor diffusion method: 1μl of 6mg/ml peptide dissolved in water was mixed with 2 μl of reservoir solution. The drop was equilibrated over 1 ml of reservoir solution containing 0.1 M sodium acetate pH 4.5 and 0.7 M hexanediol. ^{101}DSVISLS^{107} was crystallized using the hanging drop vapor diffusion method: after filtering with a 0.2μm filter, 1μL of 3 mg/mL peptide was mixed with 1 μL of reservoir solution, comprising 0.1 M MES pH 6.0, 20% PEG 6000, and 5 mM $ZnCl_2$. Peptide crystals were mounted directly onto the ends of pulled glass capillaries.

X-ray diffraction and data processing: X-ray diffraction data were collected at beamline 24-ID-E of the Advanced Photon Source, Argonne National Laboratory, Argonne, IL, USA with a wavelength of 0.8954 Å and at beamline ID13 at the European Synchrotron Radiation Facility in Grenoble, France with a wavelength of 1.0332 Å. Data were collected at 100 K with 5° oscillations.
Indexing of diffraction images was performed using the programs DENZO (2) or XDS (3) Scaling of data was performed using the program SCALEPACK (2). The merged scaled data were imported into CCP4 format with programs from the CCP4 program suite organized under the "CCP4i" interface (4). Molecular replacement solutions were found using the program Phaser (5). In the case of ^{147}GVIGIAQ^{153} the search models consisted of geometrically idealized β-strands with side chain conformations modeled as the most frequently observed rotamers defined in the graphics program COOT (6). The solution of the ^{147}GVTGIAQ^{153} (I149T) was found by Phaser (5) using the structure of GVIGIAQ as a search model. A molecular replacement solution for ^{101}DSVISLS^{107} was determined using an extended beta strand of sequence ^{101}DSVISAS^{107} after expanding dataset with SFTOOLS in the CCP4 suite (4) from $P2_1$ to P1. Crystallographic refinements were performed with the programs Refmac (7), Buster, and Phenix (8). Model building was performed with COOT (6) and illustrated with PyMOL (9). Area buried and shape complementarity were calculated with AREAIMOL (10) and SC (11), respectively.

X-ray powder diffraction of GIIGIAQ (V148I): Aggregates of GIIGIAQ (V148I) grown in 0.1 M sodium phosphate pH 2.5 were pelleted by spinning the sample for 5 minutes at 20,000 x g. The pellet was scooped with a crystallization loop. Data was collected for 5 minutes with 1° oscillations using an in-house Rigaku RAXIS-4++ image plate detector (Rigaku-FRD).

Protein expression, purification and metal removal: Human $SOD1^{WT}$ and $SOD1^{G93A}$ were expressed in the EGy118 strain of *Saccharomyces cerevisiae (S. cerevisiae)*, which lacks the endogenous yeast *sod1* gene. The proteins were purified and metals were removed as previously described in (12), except that, in the last step, 25 mM potassium phosphate, pH 7.0, 1 mM EDTA were used as dialysis buffer. After metal removal**,** $apoSOD1^{WT}$.and $apoSOD1^{G93A}$ were immediately frozen and stored in -80°C. The protein was used within two weeks of freezing. In Fig. 5, Fig. S6, Fig. S7 and Fig. S8, assays are performed with SOD1 purified from *S. cerevisiae.* We also used human SOD1 with C6A and C111S substitutions (AS-SOD1) purified from *Escherichia coli (E. coli).* AS-SOD1 has similar properties to the wild-type protein (13), but lacks the two surface exposed Cys, which can cross link to form larger oligomers (14). The plasmid with the AS-SOD1 gene was kindly provided by Becky Chan (Prof. Valentine lab). Pro mutations at positions I18P, I35P, I104P and I149P in the AS-SOD1 gene were made using QuickChange Site-Directed mutagenesis Kit (Stratagene).
Proteins (wild-type and mutants) were expressed in the *E. coli* strain BL21(DE3) in the following way. Cells transformed with pET 22b vector containing AS-SOD1 gene, were grown in LB media containing 100μg/ml ampicillin at 37°C with shaking. Cells were induced at OD_{600} ~0.6 with 1 mM IPTG. $ZnSO_4$ was added to a final concentration of 0.05mM to aid protein folding. Then, cells were grown at 32°C. After 4 hours, the cells were harvested by centrifugation for 10-15 min at 4600xg.
To release the protein from the periplasm, the cell pellet was resuspended in ice-cold 30 mM Tris-HCl pH 8, 20% sucrose (20-30ml for 1L growth media). Then, cells were stirred slowly at 4°C for 20 min. The cell slurry was spun at 10,000 × g at 4°C for 10 min and the supernatant was discarded. The cell pellet was resuspended in ice-cold water (20-30 ml for 1L growth media) and stirred slowly at 4°C for 20 min. During this step, the periplasmic proteins together with the expressed protein were released into the buffer. The cell suspension was centrifuged at 10,000xg for 10min. Ammonium sulfate was added to the supernatant which contained the expressed protein released by the double osmotic shock (0.326g ammonium sulfate per ml supernatant) and stirred at 4°C for 45min. This solution was centrifuged at 14,000xg for 30min. Then, the supernatant, containing the expressed protein, was mounted on a HiTrap Phenyl HP 5ml column (GE Healthcare). Solvent A was 2.5 M ammonium sulfate, 0.15 M sodium chloride, 0.05 M sodium phosphate, pH 7.0. Solvent B was 0.15 M sodium chloride, 0.05 M sodium phosphate, pH 7.0. Proteins were eluted by running a 100 ml gradient from 0% to 100% at 5ml/min. Finally, the protein was loaded on a size-exclusion silica G3000 column (Tosoh Bioscience). The column buffer comprised 0.1 M sodium sulfate, 25 mM sodium phosphate, and 1 mM sodium azide pH 6.5.
To remove metals from AS-SOD1 and its mutants we followed the protocol described in (12), except that, in the last step, 25 mM potassium phosphate, pH 7.0, 1 mM EDTA were used as dialysis buffer**.** Fibril formation assays were done immediately after the metal removal.

Fluorescence assays: Concentrated protein was thawed on ice and filtered through a 0.2μm filter prior to the fibril formation assay. Fibril formation assays were performed with 17 μM

apoSOD1^{WT} and apoSOD1^{G93A} in 25 mM potassium phosphate buffer, pH 7.0, 1 mM EDTA, 35 mM Tris(2-carboxyethyl)phosphine (TCEP) and 10 μM ThioflavinT. Under the conditions used, the SOD1 dimer is dissociated, so the molar concentrations of wild-type apoSOD1^{WT} and apoSOD1^{G93A} were calculated using the molecular weight of the monomer. Stock solutions of 0.4 mM ^{147}GVIGIAQ^{153} were made by dissolving lyophilized peptide in 10 mM potassium phosphate pH 7.0 with 1 mM EDTA. Stock solutions of 0.8mM ^{14}VQGIINFE^{21}, ^{33}GSIKGL^{38}, and ^{101}DSVISLS^{107} were made by dissolving the lyophilized peptide in 10mM potassium phosphate pH 7.0, 1mM EDTA. Peptides were added in the molar ratios indicated in Fig. 5A and B and Fig S6 and S7. Aggregation assays of apoAS-SOD and its Pro mutants were performed with 35 μM protein in 25mM sodium citrate pH 3.5, 1mM EDTA, 30 mM TCEP and 10 μM ThioflavinT.

Seeding experiments were done using previously formed fibrils (prepared with 25 μM protein; see above). 50 μl of the pre-formed fibrils were pipetted in a glass NMR tubes and sonicated in a water bath for 15 minutes. After sonication the fibrils were diluted twice and 2 μl were added for every 100 μl reaction volume to make 2% seed solutions (v/v).

All assays were performed in black Nunc 96-well optical bottom plates (Thermo Scientific). Teflon balls (1/8 inch in diameter) were distributed into each well of the 96-well plate. Then, 150-200 μL of solution (four replicates per sample) were pipetted into each. The plate was agitated at 300 rpm with a 3-mm rotation diameter in a Varioskan microplate reader (Thermo) at 37 °C. Fluorescence measurements were recorded every 10-15 min by using λ_{ex} = 444 nm, λ_{em} = 482 nm, with an integration time of 200 μs. Description of data normalization and plotting can be found in the Supporting Information.

Normalization of the fluorescence data: For simplicity, in Fig. 5 the mean values of ThT fluorescence are displayed. The individual values, which were used to calculate the mean signal shown in Fig. 5, were re-plotted in Fig. S6. Similarly, Figs S7 and S8 were made by plotting the individual sample replicates. In all figures, the ThT fluorescence signal was corrected for the background by subtracting the mean fluorescence signal acquired during the first one to two hours of the assay. The fluorescence was also normalized by dividing each measurement by the mean signal collected for two to four hours during which the fluorescent reading had the largest value. If one of the sample replicates had fluorescence reading close to the background, its fluorescence was normalized by dividing it by the mean fluorescence reading of the remaining replicates. The data was smoothed by substituting each data point with the average value calculated using four data points collected prior and after the point and the point itself. This is equivalent to using a central moving average with a sliding nine data point window. The normalized fluorescence signal of the peptides (^{14}VQGIINFE^{21}, ^{33}GSIKGL^{38}, ^{101}DSVISLS^{107} and ^{147}GVIGIAQ^{153}) incubated without the protein was calculated using the averaged fluorescence signal of maximum fluorescence acquired over two to three hours from the assays done with the largest peptide to protein ratios.

Transmission Electron Microscopy: Negatively stained specimens for transmission electron microscopy (TEM) were prepared by applying 5 μL of sample on hydrophilic 400 mesh carbon-coated formvar support films mounted on copper grids (Ted Pella, Inc.). The samples were allowed to adhere for 3 min, rinsed twice with distilled water and stained for 1 min with 1% uranyl acetate. Grids were examined on either a JEM1200-EX (JEOL) or T12 (FEI) microscope.

References:

1. Johnson LM, *et al.* (2012) Enhancement of alpha-helix mimicry by an alpha/beta-peptide foldamer via incorporation of a dense ionic side-chain array. *J Am Chem Soc* 134(17):7317-7320.
2. Otwinowski ZM, W. (1997) Processing of X-ray diffraction data collected in oscillation mode. *Methods Enzymol.* 276:307-326.
3. Kabsch W (1993) Automatic processing of rotation diffraction data from crystals of initially unknown symmetry and cell constants. *J. Appl. Crystallogr.* 26:795– 800.
4. Winn MD, *et al.* (2011) Overview of the CCP4 suite and current developments. *Acta Crystallogr D Biol Crystallogr* 67(Pt 4):235-242.
5. McCoy AJ, *et al.* (2007) Phaser crystallographic software. *J Appl Crystallogr* 40(Pt 4):658-674.
6. Emsley P & Cowtan K (2004) Coot: model-building tools for molecular graphics. *Acta Crystallogr D Biol Crystallogr* 60(Pt 12 Pt 1):2126-2132.
7. Murshudov GN, Vagin AA, & Dodson EJ (1997) Refinement of macromolecular structures by the maximum-likelihood method. *Acta Crystallogr D Biol Crystallogr* 53(Pt 3):240-255.
8. Adams PD, *et al.* (2010) PHENIX: a comprehensive Python-based system for macromolecular structure solution. *Acta Crystallogr D Biol Crystallogr* 66(Pt 2):213-221.
9. DeLano WL (2002) The PyMOL Molecular Graphics System. *http://www.pymol.org*.
10. Anonymous (1994) The CCP4 suite: programs for protein crystallography. *Acta Crystallogr D Biol Crystallogr* 50(Pt 5):760-763.
11. Lawrence MC & Colman PM (1993) Shape complementarity at protein/protein interfaces. *J Mol Biol* 234(4):946-950.
12. Doucette PA, *et al.* (2004) Dissociation of human copper-zinc superoxide dismutase dimers using chaotrope and reductant. Insights into the molecular basis for dimer stability. *J Biol Chem* 279(52):54558-54566.
13. DiDonato M, *et al.* (2003) ALS mutants of human superoxide dismutase form fibrous aggregates via framework destabilization. *J Mol Biol* 332(3):601-615.
14. Banci L, *et al.* (2007) Metal-free superoxide dismutase forms soluble oligomers under physiological conditions: a possible general mechanism for familial ALS. *Proc Natl Acad Sci U S A* 104(27):11263-11267.
15. Goldschmidt L, Teng PK, Riek R, & Eisenberg D (2010) Identifying the amylome, proteins capable of forming amyloid-like fibrils. *Proc Natl Acad Sci U S A* 107(8):3487-3492.

SI Figures:

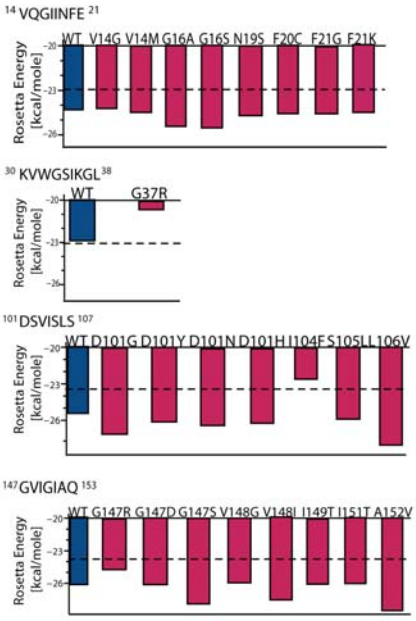

Supporting Figure S1: Mutations associated with fALS preserve the fibril-forming propensities with the exception of G37R in ^{30}KVWGSIKGL^{38} and I104F in ^{101}DSVISLS^{107}. The Rosetta energies of wild-type segments are shown in blue and the energies of segments with fALS mutations are in red. Nearly all mutant segments are predicted to form fibrils with energies below the threshold value of -23 kcal/mol (dashed line).

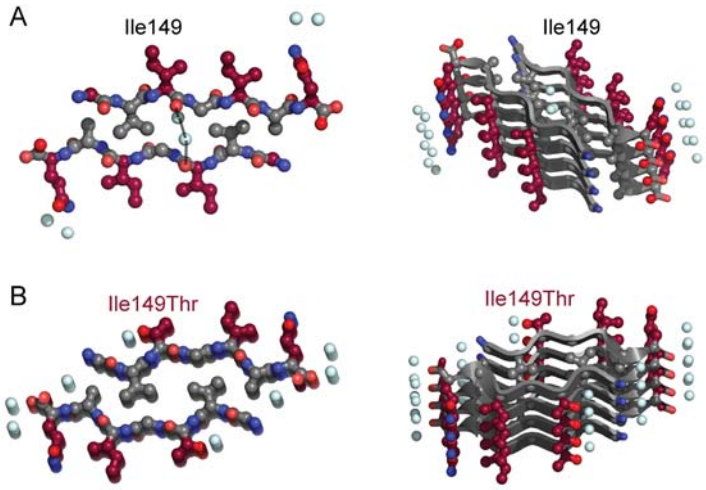

Supporting Figure S2: Wet interfaces of the steric zippers formed of ^{147}GVIGIAQ^{153} and ^{147}GVTGIAQ^{153} (I149T). A) Val148 of the wild-type segment is intercalated between residues Gly150 and Val151 of the mating β-sheet. The interaction between the two β-sheets is mediated through hydrogen bonds between Gly150 from the mating sheet interface and two water

molecules . **B)** In contrast, Val148 of I149T is shifted by about 2Å to face Gly150 of the mating β-sheet and there are no water molecules between the β-sheets.

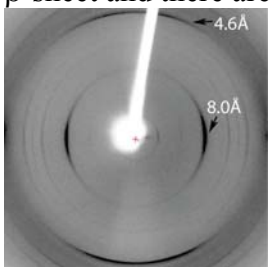

Supporting Figure S3: The V148I mutation in the ^{147}GVIGIAQ^{153} segment does not perturb the propensity of the mutant peptide to form fibril-like aggregates. The x-ray diffraction pattern of ^{147}GIIGIAQ^{153} (V148I) rod-like aggregates grown at pH 2.5 displays a cross-β diffraction pattern typical of amyloid fibrils, with a meridional reflection at 4.7 Å and an equatorial reflection at 8.0 Å.

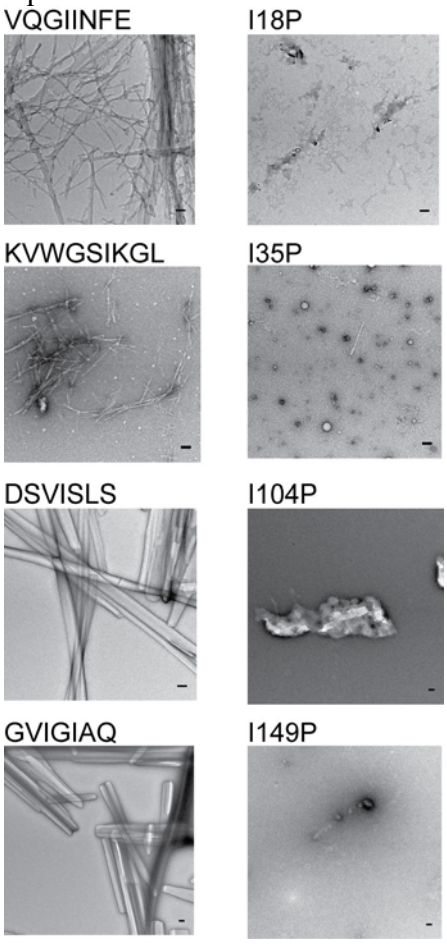

Supporting Figure S4: Single Pro mutation is sufficient to inhibit the aggregation of SOD1 fibril forming peptides. All SOD1 segments with high propensity to form fibrils formed fibril-like aggregates (left panels). Peptides with Pro substitutions in the middle of the same segments formed amorphous aggregates, which lacked the typical amyloid-like fibril morphology (right

panels). Based on this data, we inferred that Pro mutations would block the fibril formation of each SOD1 fibril-forming segment in the context of the full-length protein.

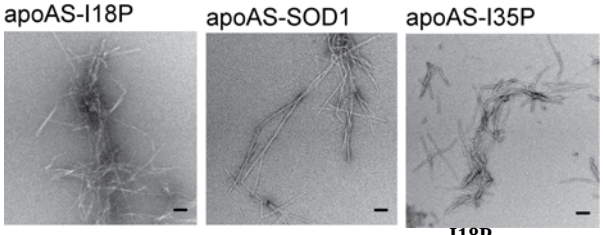

Supporting Figure S5: apoSOD1^{I18P} and apoSOD1 ^{I35P} formed aggregates with morphology similar to apoSOD1^{WT}. TEM was used to assess whether segments ^{14}VQGIINFE^{21} and ^{30}KVWGSIKGL^{38} are important for fibril formation of the full-length protein. Proteins with I18P and I35P substitutions found to block the aggregation of segments ^{14}VQGIINFE^{21} and ^{30}KVWGSIKGL^{38}, formed fibrils with similar morphology to wild-type protein. Based on this, we can conclude that in the conditions tested, ^{14}VQGIINFE^{21} and ^{30}KVWGSIKGL^{38} are auxiliary rather than the building segments of the fibril core.

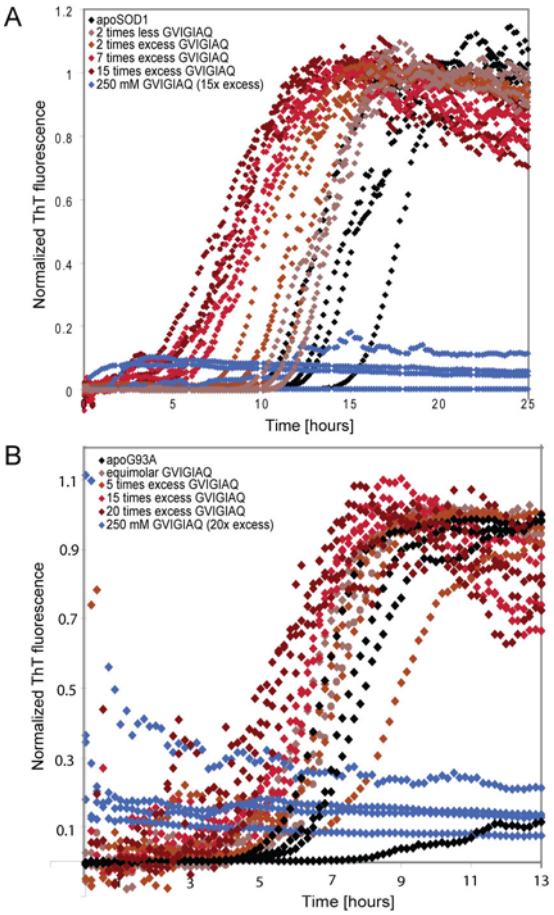

Supporting Figure S6: The C-terminal segment ^{147}GVIGIAQ^{153} accelerates the fibril formation of full-length apoSOD1. The individual fluorescence curves representing each of the four sample replicates, which were used to calculate the average fluorescence shown in Fig. 5, are plotted. The C-terminus peptide ^{147}GVIGIAQ^{153} accelerates the fibril formation of both apoSOD1^{WT} **A)** and apoSOD1^{G93A} **B).**

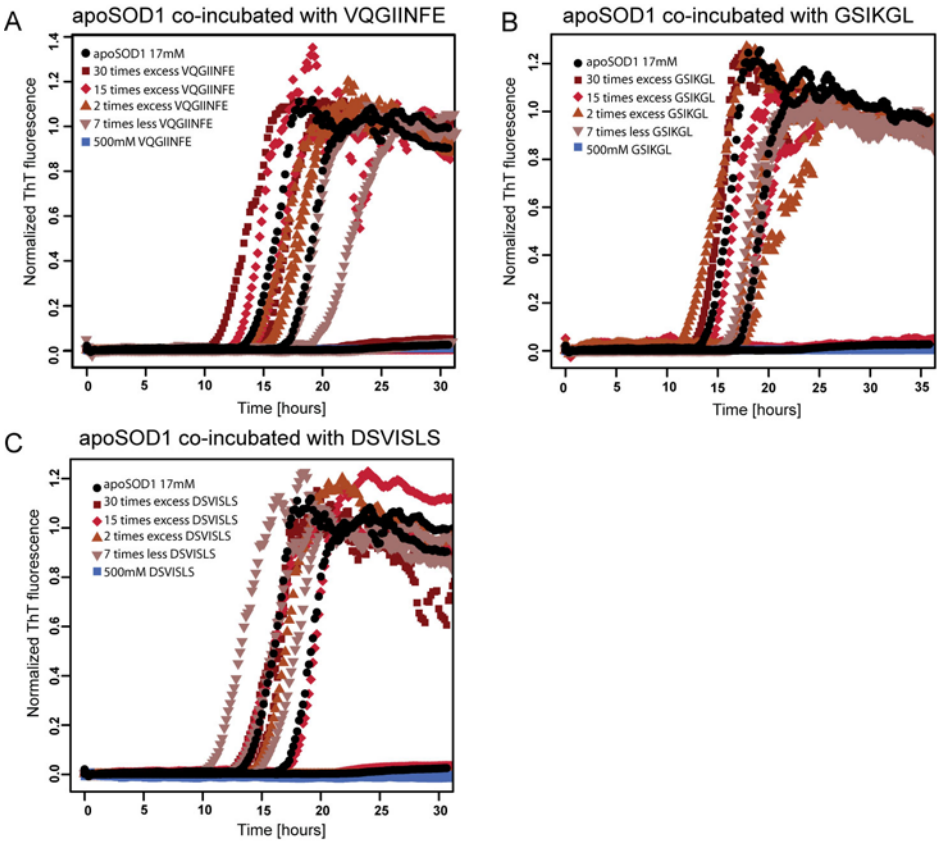

Supporting Figure S7: ^{14}VQGIINFE^{21}, ^{33}GSIKGL^{38} and ^{101}DSVISLS^{107} do not nucleate apoSOD1^{WT} fibril formation. A) ^{14}VQGIINFE^{21} does not alter apoSOD1 fibril formation when added at 30 times, 15 times, 2 times more or 2 times less than the full-length protein. Similarly, segments ^{33}GSIKGL^{38} **B)** and ^{101}DSVISLS^{107} **C)** do not affect fibril formation of the full-length protein. While these segments show no effect on protein aggregation, it is possible that under different experimental conditions these segments may become accessible for self-association. Each reaction was performed in triplicate and is represented by curves that are the same color.

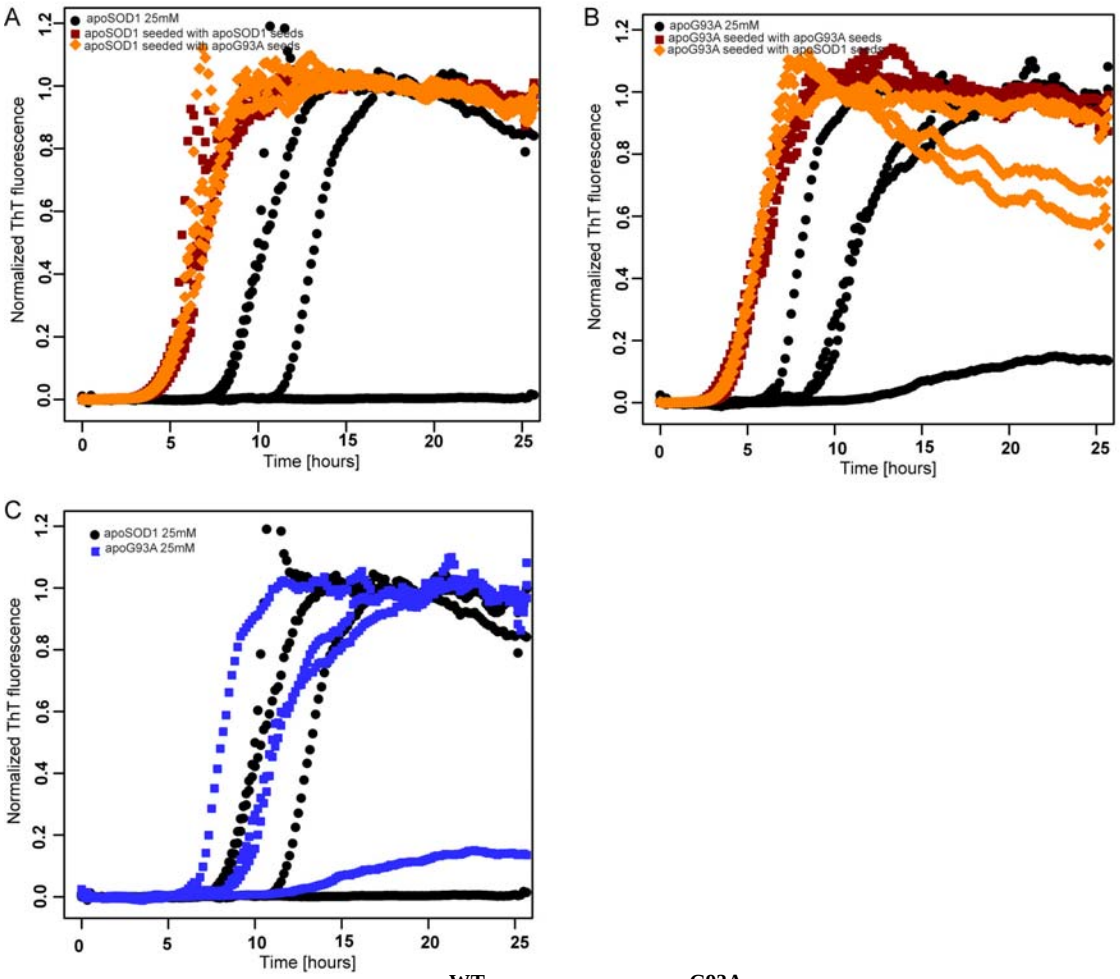

Supporting Figure S8: apoSOD1^{WT} and apoSOD1 ^{G93A} can cross-seed fibril formation. A) The fibril formation of apoSOD1^{WT} is seeded as efficiently with apoSOD1 ^{G93A} nuclei as with seeds formed with the wild-type protein. **B)** The reverse it also true. The fibril formation apoSOD1^{G93A} can be cross-seeded with apoSOD1^{WT} nuclei. **C)** apoSOD1^{WT} and apoSOD1 ^{G93A} show similar rates of aggregation.

Supporting Table S1: The effect of fALS-associated mutations on the fibril formation propensity of the SOD1 segments predicted to form fibrils: To compare the fibril formation propensity between segments longer than six residues, we calculated the average Rosetta energy for each sequence cluster (15). The mutated residues are shown in bold and underlined. The segments with Rosetta energies larger than the threshold (-23 kcal/mol) are shown in italic. ^{30}KVWGSIKGL^{38}, has an averaged Rosetta energy slightly above the threshold energy due to the presence of two six-residue segments with unfavorable fibril formation energies. We studied this segment because two six-residue segments that are part of ^{30}KVWGSIKGL^{38} are predicted to form fibrils.

Peptide name	**Mutation**	**Rosetta Energy [kcal/mole]**
Cluster: VQGIINFE	**Wild-type**	**-24.4: average**
VQGIIN		-24.2
QGIINF		-24.9
GIINFE		-24.0
Cluster: GQGIINFE	**V14G**	**-24.4: average**
GQGIIN		-24.4
QGIINF		-24.9
GIINFE		-24.0
Cluster: MQGIINFE	**V14M**	**-24.3: average**
MQGIIN		-24.0
QGIINF		-24.9
GIINFE		-24.0
Cluster: VQSIINFE	**G16S**	**-25.6: average**
VQ**S**IIN		-27.0
Q**S**IINF		-25.5
SIINFE		-24.2
Cluster: VQAIINFE	**G16A**	**-25.4: average**
VQ**A**IIN		**-25.9**
Q**A**IINF		**-25.4**
AIINFE		**-24.8**
Cluster: VQGIISFE	**N19S**	**-24.8: average**
VQGII**S**		**-25.3**
Q**G**II**S**F		**-24.4**
GII**S**FE		**-24.8**
Cluster: VQGIINCE	**F20C**	**-24.6: average**
VQ**G**IIN		-24.2
Q**G**IIN**C**		-24.6
GIIN**C**E		-24.4
Cluster: VQGIINFG	**E21G**	**-24.5: average**
VQ**G**IIN		-24.2
QGIINF		-24.8
GIINF**G**		-24.6
Cluster: VQGIINFK	**E21K**	**-24.5:average**
VQ**G**IIN		-24.2
QGIINF		-24.8

GIINF**K**		-24.5
Cluster: KVWGSIKGL KVWGSI VWGSIK WGSIKG GSIKGL	**Wild-type**	***-22.9: average*** -24.0 *-21.7* *-20.8* -25.0
Segment: KVWGSIK**R**L KVWGSI VWGSIK WGSIK**R** GSIK**R**L	**G37R**	***-20.9: average*** -24.0 *-21.7* *-17.4* *-20.4*
Cluster: DSVISLS DSVISL SVISLS	**Wild type**	**-25.5 average** -25.3 -25.9
Cluster: GSVISLS **G**SVISL SVISLS	**D101G**	**-26.5 average** -27.1 -25.9
Cluster: YSVISLS **Y**SVISL SVISLS	**D101Y**	**-25.4 average** -24.8 -25.9
Cluster: HSVISLS **H**SVISL SVISLS	**D101H**	**-25.6 average** -25.4 -25.9
Cluster: NSVISLS **N**SVISL SVISLS	**D101N**	**-25.7: average** -25.5 -25.9
Cluster: DSVFSLS DSV**F**SL SV**F**SLS	**I104F**	***-22.2: average*** -20.5 -23.9
Cluster: DSVILLS DSVI**L**L SVI**L**LS	**S105L**	**-25.2: average** -23.9 -26.4
Cluster: DSVISVS DSVISV SVISVS	**L106V**	**-27.1: average** -26.4 -27.8
Cluster: GVIGIAQ GVIGIA VIGIAQ	**Wild type**	**-26.1: average** -27.1 -25.1
Cluster: RVIGIAQ **R**VIGIA VIGIAQ	**G147R**	**-23.4: average** *-21.6* -25.1
Cluster: DVIGIAQ **D**VIGIA VIGIAQ	**G147D**	**-24.7: average** **-24.2** **-25.1**
Cluster: SVIGIAQ **S**VIGIA	**G147S**	**-26.0: average** **-26.9**

VIGIAQ		**-25.1**
Cluster: G<u>G</u>IGIAQ G<u>**G**</u>IGIA <u>**G**</u>**IGIAQ**	**V148G**	**-24.4: average** -25.1 -23.7
Cluster: G<u>I</u>IGIAQ G<u>**I**</u>IGIA <u>**I**</u>IGIAQ	**V148I**	**-25.8: average** -27.1 -24.4
Cluster: GV<u>T</u>GIAQ GV<u>**T**</u>GIA VTGIAQ	**I149T**	**-24.5: average** -24.7 -24.3
Cluster: GVIG<u>T</u>AQ GVIG<u>**T**</u>A VIG<u>**T**</u>AQ	**I151T**	**-24.5: average** -25.5 -23.5
Cluster: GVIGIVQ GVIGI<u>**V**</u> VIGI<u>**V**</u>Q	**A152V**	**-26.7: average** **-27.8** **-25.5**

Supporting Table S2: Comparison of the steric zippers formed by ^{101}DSVISLS^{107}, ^{147}GVIGIAQ^{153}, and fALS mutant ^{147}GVTGIAQ^{153} (I149T).

Segment Sequence	Shape complementarity of dry interface	Area buried Å^2 dry interface	Sheet-to-sheet Distance dry interface Å	Shape complementarity of wet interface	Area buried Å^2 wet interface	Sheet-to-sheet Distance Wet interface Å
GVIGIAQ	0.81	419	11.4	0.74	462	6.7
GV<u>T</u>GIAQ	0.94	549	9.8	0.85	540	6.7
DSVISLS	0.77	430	9.5	0.77	430	9.5

Supporting Table S3: Statistics for data collection, processing and refinement of ^{147}GVIGIAQ^{153}, ^{147}GVTGIAQ^{153} (I149T) and ^{101}DSVISLS^{107}.

Data Collection	**GVIGIAQ**	**GVTGIAQ**	**DSVISLS**
Space Group	C2	C2	$P2_1$
Resolution (Å)	1.9	1.3	1.4
Unit Cell Dimensions			
a (Å)	50.13	47.79	4.795
b (Å)	4.84	4.79	45.51
c (Å)	18.14	17.69	11.15
β (°)	99.5	109.4	100.4
Measured Reflections	1001	4551	2644
Unique Reflections	415	1053	717
Overall Redundancy	2.4	4.3	3.7
Last Shell Redundancy	2.4	2.4	1.4
Overall Completeness (%)	95.2	95.7	73.6
Last Shell Completeness (%)	89.2	81.6	28.4
Overall R_{sym}	14.4	12.8	18.6
Last Shell R_{sym}	20.6	26.8	16.6
Overall I/σ(I)	6.3	7.3	6.1
Last shell I/σ(I)	4.8	3.6	3.7
Refinement			
R_{work}	23.2	20.18	18.7
R_{free}	24.8	23.32	22.8
r.m.s.d. bond length (Å)	0.010	0.004	0.006
r.m.s.d. bond angle (°)	1.32	1.064	0.92
Number of protein atoms	46	45	50
Number of solvent atoms	3	4	4
Average B factor of protein atoms	16.32	6.01	19.07